

高效 MAG 焊接熔滴过渡行为及交变磁场控制试验分析

樊 丁^{1,2}, 郑发磊¹, 肖 磊¹, 陈克选^{1,2}

(1. 兰州理工大学 材料科学与工程学院, 兰州 730050;

2. 兰州理工大学 省部共建有色金属先进加工与再利用国家重点实验室, 兰州 730050)

摘 要: 探索更加高效的焊接方法和工艺是当前国际焊接界一个热点课题, 而增大焊接电流和焊丝伸出长度可直接提高 MAG 焊接效率. 文中对商用 MAG 焊机进行改造, 使送丝速度达到 50 m/min, 焊接电流提升至 500 A 以上, 以进一步提高焊接效率. 但是熔滴旋转射流过渡的形成, 导致电弧不稳, 飞溅增大, 因而采用外加交变磁场来改善电弧形态和熔滴过渡行为. 通过焊接工艺试验, 分析了焊接电流对焊接飞溅率和金属蒸发速率的影响规律, 研究了交变磁场对熔滴过渡行为和焊缝成形的作用. 结果表明, 外加低频交变磁场可以有效提高大电流下电弧挺度和稳定性, 缩短液流束长度, 减小液尖偏斜程度, 进而改善焊缝成形, 大幅度提高焊接效率.

关键词: 熔滴过渡行为; 旋转射流过渡; 金属蒸发速率; 交变磁场

中图分类号: TG 403 **文献标识码:** A **doi:** 10.12073/j.hjxb.2019400118

0 序 言

统计显示: 2015 年全球粗钢产量由 2006 年的 12.5 亿吨增加至 16.2 亿吨; 中国粗钢产量由 4.2 亿吨增加至 8.0 亿吨, 十年增幅高达 90.5%, 2017 年同样高达 8.3 亿吨. 而全球钢产量的 40%~60% 需要通过焊接加工来实现其应用, 因此研究高效焊接技术已成为当前国际焊接领域的热点课题之一.

国内外焊接学者提出了不同的高效焊接工艺. 例如 T.I.M.E. 焊接工艺^[1], 通过加入特殊的四元保护气体 (O₂, CO₂, He, Ar), 使旋转射流过渡过程趋于稳定, 同时飞溅减少, 焊缝成形得到改善; 双丝 GMAW 焊接和激光-MIG 复合焊等^[2-3], 也显著提高了焊接效率. 但由于设备要求高或工艺参数复杂等缺点限制了其使用范围^[4].

MAG 焊因具有焊接过程稳定、焊接质量高的特点在生产中具有广泛的应用. 提高 MAG 焊焊丝的熔化速率是实现高效焊接重要的因素^[5], 但是当焊接电流超过临界电流时, 熔滴过渡将由轴向射流过渡变为旋转射流过渡. 这种过渡方式的电弧极不稳定, 金属飞溅严重, 焊缝成形差, 不能用于焊接生

产中^[6]. 因此极大限制了焊接效率的进一步提高. 近年来, 有学者尝试在传统的 GMAW 焊接中施加外部磁场控制焊接过程稳定性^[7-8]. 陈树君等人^[9]在 MAG 电弧外加直流纵向磁场, 试验发现直流磁场可以使旋转射流过渡的稳定性得到改善. 常云龙等人^[10]在 CO₂ 焊外加纵向低频磁场, 改变了电弧形态, 降低了焊接飞溅. 文中研究通过对商用 MAG 焊机改造, 大幅提高了焊丝送丝速度和焊接效率, 并通过施加交变磁场, 控制高效 MAG 焊接时的熔滴过渡形式、电弧形态及焊缝成形, 以便进一步提升焊接效率.

1 试验方法

1.1 试验系统

如图 1 所示, 试验系统主要包括焊接电源、磁控装置 (包括励磁电源和激磁线圈) 和摄像系统.

试验采用 MEGMEET 公司型号为 Artsen CM500C 的焊机, 经改造送丝速度由 22 m/min 提高到 50 m/min. 试件为 Q235 低碳钢板 (尺寸 250 mm × 80 mm × 10 mm), 焊丝直径为 1.2 mm, 型号为 H08 Mn2SiA, 保护气体为 Ar(20 L/min) + CO₂(4 L/min). 焊接采用平板堆焊的方式, 并在焊接过程中用 Olympus i-speed 3 高速相机对熔滴过渡行为及电弧形态进行拍摄, 图像采集速率为 7 500 帧/秒.

收稿日期: 2018 - 02 - 11

基金项目: 国家自然科学基金资助项目 (51775256); 甘肃省基础研究创新群体计划资助项目 (17JR5RA107); 甘肃省高校协同创新团队项目 (2017C-07)

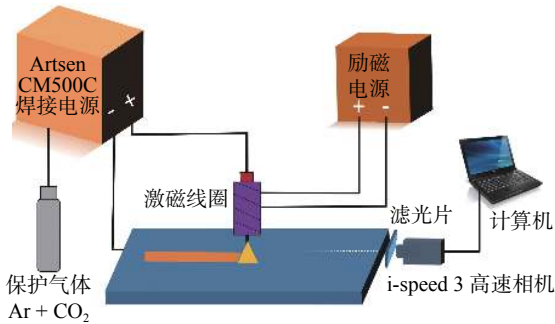


图 1 磁控 MAG 焊接试验系统示意图

Fig. 1 MAG welding system controlled by magnetic field

1.2 激磁线圈及磁场的作用原理

为将交变磁场施加到焊接电弧中,设计了一套基于控制芯片 SG3525 为核心的多功能逆变磁控装置,磁场由安装在焊枪上的激磁线圈产生.如图 2 所示,试验采用的线圈匝数为 120 匝,线圈内装嵌壁厚为 4.5 mm 的铁芯.外加磁场的磁场强度和频率均可通过磁控装置进行调控,也可通过高精度科研型特斯拉计对磁场进行测量.磁力线以焊丝轴线为中心成轴对称分布,与工件表面相垂直.纵向磁场加入焊接电弧之中,与焊接电流相互作用,产生洛伦兹力,从而控制焊接电弧和熔滴过渡行为.



图 2 激磁线圈结构

Fig. 2 Structure of excitation coil

2 试验结果与分析

2.1 焊接电流和焊丝伸出长度对焊丝熔化速率的影响

提升焊丝的熔化速率是进一步提高焊接效率的关键.当直流反接,焊丝确定时,焊接电流 I 和焊丝伸出长度 L_m 是影响焊丝熔化速率的主要因素.因此试验测试了随焊接电流增加,不同焊丝伸出长

度下的焊丝熔化速率.焊丝熔化速率与焊接电流和焊丝伸出长度的关系如图 3 所示.

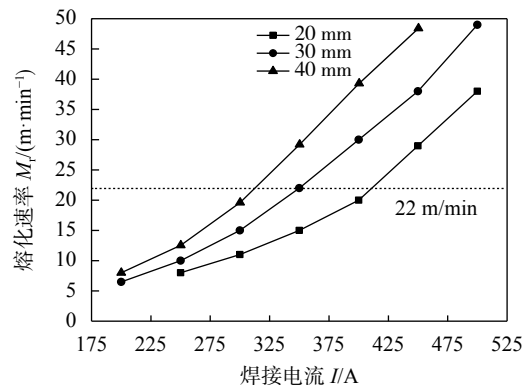


图 3 焊丝熔化速率与焊接电流和焊丝伸出长度的关系

Fig. 3 Wire melting rate as a function of welding current and extension length

从图 3 可以看出,相同的焊丝伸出长度,增大焊接电流,焊丝熔化速率显著升高;焊丝伸出长度越长,熔化速率也越高.目前国内商用 MAG 焊机最大送丝速度为 22 m/min,其对应的焊接电流为 400 A 左右.为进一步提高焊接效率,对焊机进行改造,使送丝速度达到 50 m/min,焊接电流延伸到 500 A 以上.而且当焊接电流在 400 ~ 500 A 以上,焊丝伸出长度 20 ~ 40 mm 范围内焊接时,焊丝熔化速率较商用 MAG 焊机大幅提升,可将焊接效率提高一倍以上.因此增大焊接电流和焊丝伸出长度,是提升焊接效率的最直接途径.

2.2 熔滴旋转射流过渡的形成分析

增大焊接电流和焊丝伸出长度可大幅度提高焊接效率,但超过临界值后,熔滴过渡将由射流过渡变为旋转射流过渡形式.图 4 为射流过渡和旋转射流过渡熔滴过渡行为及电弧亮区形态.

如图 4a 所示,熔滴射流过渡时,电弧亮区呈锥形,焊丝末端金属液尖呈现铅笔尖状,熔滴在等离子流力作用下沿焊丝轴向高速向熔池过渡.当焊接电流和焊丝伸出长度增大后,如图 4b 所示,金属液尖在强电磁收缩力作用下进一步拉长形成细长的液流束.液流束过热产生大量金属蒸气,而金属蒸气的电离电压要低于保护气体 (Ar 和 CO_2) 的电离电压,所以电弧亮区向下移动露出液尖,只包围液流束燃烧,这样就使阳极斑点形成在液尖端点.细长液流束由于质量小在焊接过程中容易受到干扰使其偏离焊丝轴线,焊接电弧也随之偏斜,金属液尖便在斑点力及熔滴高速喷出反作用力的作

用下偏离焊丝轴线, 这就导致液尖所受合力偏离焊丝轴线, 提供了液尖绕焊丝轴线做旋转运动的向心力, 液尖高速旋转并带动液流束与焊接电弧旋转. 而

且液流束断裂抛向四周产生焊接飞溅, 从而形成熔滴旋转射流过渡. 焊丝伸出长度越长, 液尖越容易偏离焊丝轴线, 也越容易形成旋转射流过渡.

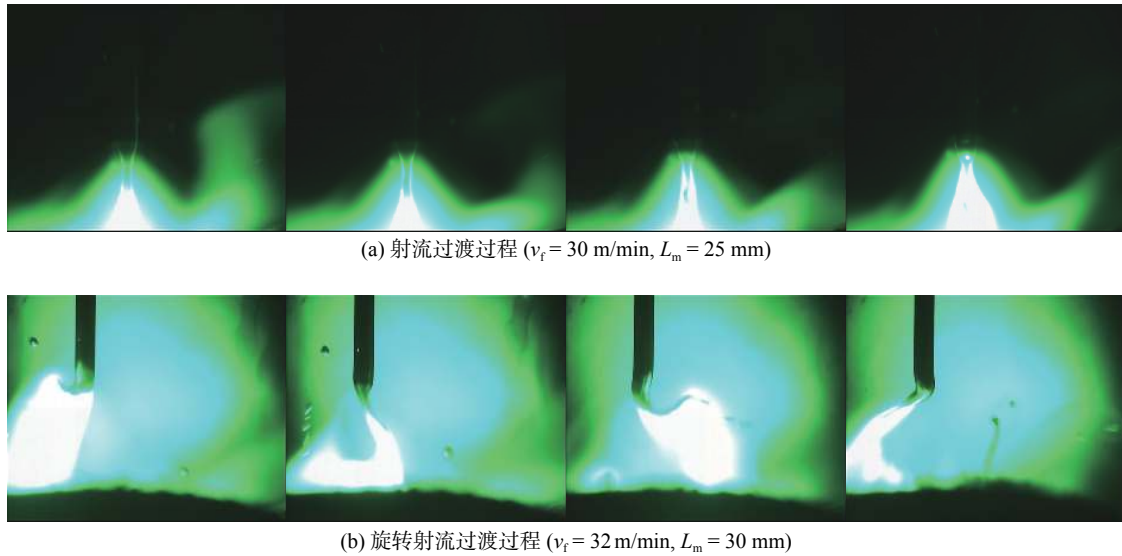


图 4 熔滴过渡行为及电弧形态
Fig. 4 Droplet transfer behavior and arc shape

2.3 焊接飞溅与金属蒸发的测试分析

为提高焊接效率, 既要求焊丝的熔化速率高, 又得保证焊丝的熔敷速率. 因此对不同熔滴过渡下的焊接飞溅率 φ 和蒸发速率 R_e 进行测试分析.

试验中认定焊丝的损失量是飞溅与蒸发两部分的总和. 利用飞溅收集装置对焊接过程中产生的焊接飞溅进行收集, 并且已知焊丝总的使用量, 就可用公式 (1) 和式 (2) 计算各过渡形式下的飞溅率和蒸发速率, 即

$$\varphi = \frac{M_3}{M_1} \times 100\% \quad (1)$$

$$R_e = \frac{M_1 - M_2 - M_3}{t} \quad (2)$$

式中: 式中 M_1 为焊丝使用量; M_2 为焊丝熔敷量; M_3 为飞溅量; t 为焊接时间.

根据计算结果, 绘制飞溅率和蒸发速率随焊接电流的变化曲线, 如图 5 所示. 图 5 中, 焊接电流与电压较小时, 熔滴过渡方式为短路过渡 (a-b), 该过程中熔滴与熔池接触形成短路液桥, 飞溅率较大; 当焊接电流增大到喷射过渡区间内时 (c-d), 焊接过程稳定, 飞溅极少, 正常的射流过渡飞溅率仅为 1% 左右; 当焊接电流继续增大, 且焊丝伸出长度较长时, 由于熔滴旋转射流过渡的形成, 和射流过渡相比, 飞溅率在 d 点后突然增大到 12% 以上. 而且

在旋转射流过渡区间内 (e-f), 焊接飞溅率始终在 12% ~ 14% 范围内变化. 但射流过渡时, 由于焊丝端部液态金属横截面积较小, 过热形成较大金属蒸发. 随电流增大, 电弧温度继续升高, 到旋转射流过渡时金属蒸发速率将继续增大.

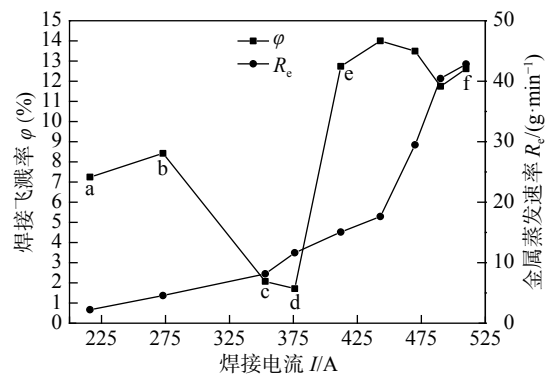


图 5 飞溅率和蒸发速率与焊接电流的关系
Fig. 5 Spatter rate and metal evaporation rate as function of welding current

由图 5 可以得出短路过渡时, 飞溅率较大, 随着焊接电流增大, 射滴过渡和射流过渡时, 飞溅率降低, 旋转射流过渡时又突然增大到一定范围内, 与熔滴过渡模式有关, 而金属蒸发速率却不受熔滴过渡模式的影响, 只与电弧温度有关, 随着焊接电流的增大, 变化趋势持续上升. 因此需采用有效控

制措施,使旋转射流过渡时电弧与熔滴过渡趋于稳定,减小焊丝损失,焊缝成形良好.

2.4 交变磁场对焊接过程的作用

大电流、大焊丝伸出长度焊接时熔滴旋转射流过渡的形成使焊接飞溅率和蒸发速率显著升高,要最终实现高效焊接,采用施加交变磁场的措施,研究其对熔滴过渡行为及焊缝成形的作用. 试验参数如表1所示.

表1 交变磁场控制 MAG 焊接试验参数

Table 1 MAG welding parameters controlled by alternating magnetic field

焊接电流 I/A	电弧电压 U/V	送丝速度 $v_f/(m \cdot \min^{-1})$	焊丝伸出长度 L_m/mm	焊接速度 $v_w/(m \cdot \min^{-1})$
450	50	35	30	0.78

按表1参数施焊形成旋转射流过渡,通过磁控装置施加频率为60 Hz、激磁电流为4 A的交变磁场,通过测量距离线圈端部30 mm处磁场有效值为19.9 Gs. 施加磁场前后焊接时熔滴过渡行为和焊缝成形如图6和图7所示.



(a) 熔滴过渡行为



(b) 焊缝成形

图6 无磁场时熔滴过渡行为及焊缝成形

Fig. 6 Droplet transfer behavior and weld appearance without magnetic field

无磁场焊接时熔滴旋转射流过渡极不稳定,从图6a可以看出,焊丝末端金属液尖拉长形成细长的近似螺旋线液流束. 由于液流束在液尖带动下进行高速旋转的非轴向过渡,旋转频率高达500 Hz,液流束破断后粘附在焊缝两侧,形成严重焊接飞溅,表面不均匀,成形较差,如图6b所示. 而且焊接电弧分散,作用在工件的面积较大,熔深较浅. 利用

液流束和电弧偏离焊丝轴线使焊接电流有径向分量和周向电流,且都与纵向磁场相垂直的条件,施加交变磁场,电流与磁场作用产生洛伦兹力,且该力随激磁电流变化改变方向,以此来减缓液流束和电弧不稳定的运动状态. 施加60 Hz交变磁场后液流束及电弧旋转方向来回转变,直到达到如图7a所示的较稳定状态,液流束长度缩短,而且液尖与焊丝轴线夹角减小,熔滴以直线形过渡. 可以认为施加的低频磁场赋予焊接电弧大的挺度和稳定性,电弧由不规则偏斜变为钟罩状电弧,电弧形态的变化增大阳极斑点的受力面积,减弱了金属蒸气对液尖的反作用力,减缓了液尖的偏斜程度,等离子流力重新成为熔滴过渡主要作用力,促使液态金属轴向过渡. 如图7b所示,施加磁场后焊缝成形均匀,飞溅显著减少,而且熔深由3.1 mm增加到5.0 mm.



(a) 熔滴过渡行为



(b) 焊缝成形

图7 施加60 Hz磁场时熔滴过渡行为及焊缝成形

Fig. 7 Droplet transfer behavior and weld appearance with 60 Hz alternating magnetic field

常规MAG焊的送丝速度上限为22 m/min,而外加60 Hz低频磁场后在35 m/min的送丝速度下对熔滴过度行为及焊缝成形进行了有效的改善,可稳定焊接. 只需施加相匹配的交变磁场参数,就可在保证焊接质量的前提下,在更高效的焊接参数下稳定焊接,大幅度提高MAG焊焊接效率.

3 结 论

(1) 增大焊接电流和焊丝伸出长度显著提高焊丝的熔化速率,是提升焊接效率的最直接途径.

(2) 液尖在斑点力及熔滴高速喷出反作用力作用下偏离焊丝轴线高速旋转, 并带动液流束与电弧旋转. 焊丝伸出长度越长, 液尖越容易偏离焊丝轴线, 越容易形成旋转射流过渡.

(3) 飞溅率大小与熔滴过渡模式密切相关; 而蒸发速率却不受熔滴过渡模式的影响, 与电弧温度有关, 随焊接电流增大, 蒸发速率持续上升.

(4) 施加低频交变磁场可有效改善熔滴旋转射流过渡及其电弧形态的稳定性, 减少焊接飞溅, 改善焊缝成形.

参考文献:

- [1] Lahnsteiner R. The T.I.M.E. process-an innovative MAG welding process[J]. *Welding Review International*, 1992, 2: 17 - 20.
- [2] Moinuddin S Q, Kapil A, Kohama K, *et al.* On process-property interconnection in anti-phase synchronized twin-wire GMAW of low carbon steel[J]. *Science and Technology of Welding and Joining*, 2016, 21(6): 452 - 459.
- [3] Zhan X H, Gao Q Y, Gu C, *et al.* The porosity formation in the laser-MIG hybrid welded joint of invar alloy[J]. *Optics and Laser Technology*, 2017, 95(10): 86 - 93.
- [4] 林三宝, 范成磊, 杨春丽. 高效焊接方法 [M]. 北京: 机械工业出版社, 2011.
- [5] Suban M, Tusek J. Dependence of melting rate in MIG/MAG welding on the type of shielding gas used[J]. *Journal of Materials Processing Technology*, 2001, 119: 185 - 192.
- [6] 包晔峰, 周 昀, 吴毅雄, 等. 大电流 MAG 焊旋转喷射过渡中的熔滴失稳分析 [J]. *焊接学报*, 2003, 24(6): 73 - 76.
Bao Yefeng, Zhou Yun, Wu Yixiong, *et al.* Instant unstable phenomenon of rotational spray transfer in high-current MAG welding[J]. *Transactions of the China Welding Institution*, 2003, 24(6): 73 - 76.
- [7] Kap P, Suoranta R, Martikainen J. Advanced gas metal arc welding processes[J]. *The International Journal of Advanced Manufacturing Technology*, 2013, 67(1-4): 655 - 674.
- [8] Chang Yunlong, Liu Xiaolong, Lu Lin. Impacts of external longitudinal magnetic field on arc plasma and droplet during short-circuit GMAW[J]. *International Journal of Advanced Manufacturing Technology*, 2014, 70(9-12): 1543 - 1553.
- [9] 陈树君, 王 军, 王会霞, 等. 纵向磁场作用下的旋转射流过渡的机理 [J]. *焊接学报*, 2005, 26(3): 45 - 49.
Chen Shujun, Wang Jun, Wang Huixia, *et al.* Principle of rotating transfer undergoing longitudinal magnetic field control[J]. *Transactions of the China Welding Institution*, 2005, 26(3): 45 - 49.
- [10] 常云龙, 李海涛, 梅 强, 等. 外加纵向磁场对 CO₂ 焊接短路液桥的影响 [J]. *沈阳工业大学学报*, 2015, 37(6): 624 - 628.
Chang Yunlong, Li Haitao, Mei Qiang, *et al.* Influence of external longitudinal magnetic field on short circuit liquid bridge of CO₂ welding[J]. *Journal of Shenyang University of Technology*, 2015, 37(6): 624 - 628.

第一作者简介:樊丁, 男, 1961 年出生, 教授, 博士研究生导师. 主要从事焊接物理、焊接智能控制以及激光加工等方面的研究. 发表论文 250 余篇. Email: fand@lut.cn

MAIN TOPICS, ABSTRACTS & KEY WORDS

Droplet transfer behavior and alternating magnetic field controlled experimental study of high efficiency MAG welding

FAN Ding^{1,2}, ZHENG Falei¹, XIAO Lei¹, CHEN Kexuan^{1,2} (1. School of Materials Science and Engineering, Lanzhou University of Technology, Lanzhou 730050, China; 2. State Key Laboratory of Advanced Processing and Recycling of Non-Ferrous Metals, Lanzhou University of Technology, Lanzhou 730050, China). pp 1-5

Abstract: Developing more efficient welding methods and processes is a hot topic in the international welding industry, and increasing welding current and extension length is a direct approach to improve melting efficiency of MAG welding. Through improving commercial MAG welding machine, wire feeding speed can reach 50 m/min, and the welding current is up to 500 A or more so as to further enhance welding efficiency. But the formation of rotating spray transfer of droplet, resulting in welding arc instability and lots of spatters, thus an alternating magnetic field is applied to control the arc morphology and droplet transfer behavior. With the welding experiment, the influence of welding current on spatter rate and metal evaporation rate was analyzed and the droplet transfer behavior and weld appearance under alternating magnetic field was studied. The results show that under high welding current with low frequency magnetic field can effectively enhance the arc stiffness and stability, shorten the length of liquid stream and reduce the deflection of fluid tip, improve the weld appearance, and then greatly increase the welding efficiency.

Key words: droplet transfer behavior; rotating spray transfer; metal evaporation rate; alternating magnetic field

Microstructural features of underwater wet friction taper plug welded joints for X52 pipeline steel

XIONG Junzhen, YANG Xinqi, LIN Wei, LIU Kaixuan (Tianjin University, Tianjin 300072, China). pp 6-12

Abstract: The experiments of underwater wet friction taper plug welding were performed on API 5L X52 pipeline steel. The microstructure of joints with different welding parameters was observed by optical and scanning electron microscope, and the effects of welding parameters on microstructure were analyzed. The results show that the joints can be divided into forged zone (FZ), final frictional plane (FFP), shear deformation zone (SDZ), bonding zone (BZ) and heat-affected zone (HAZ). The SDZ presents layered structure containing coarse grains, and the microstructure of welds is extremely inhomogeneous. The axial force has a greater

impact on microstructure of welds compared with rotational speed. The microstructure of underwater wet friction taper plug welded joint has a big difference with that of traditional friction welded joints which is characterized by fine-grained microstructure. These behaviors are caused by the welds mainly consisting of shear deformation zone during "closed mode" friction welding.

Key words: friction taper plug welding; X52 pipeline steel; welding parameters; microstructure

7A52 aluminum alloy VPPA-MIG hybrid welding residual stress testing based on elastic modulus variation

GAN Shiming^{1,2}, HAN Yongquan¹, CHEN Furong¹, LI Xiaofei¹ (1. Materials Forming Key Laboratory, Inner Mongolia University of Technology, Hohhot 010051, China; 2. College of Mechanical Engineering, Inner Mongolia University of Technology, Hohhot 010051, China). pp 13-17,23

Abstract: A residual stress testing system based on hole-drilling method was designed by virtual instrument and NI data acquisition card to analyze the welding residual stress distribution for 7A52 aluminum alloy plates after the process of VPPA-MIG hybrid welding. To reduce the impact of elastic modulus error on the final measurement results, the elastic modulus is derived from curve that is fit to data measured in different hybrid welded joint areas. The experiment of VPPA-MIG welding residual stress measurement was carried out on 10 mm thick 7A52 aluminum alloy plates. The results show that the distribution of residual stresses on two sides of weld is basically symmetrical along the weld center. Maximum tensile stresses exist in the fusion zone, and the maximum transverse residual stress σ_y and the maximum longitudinal residual stress σ_x are 118 and 223 MPa, respectively. From fusion zone to heat affected zone, residual stresses are all tensile stresses, which become smaller gradually and are higher than the residual stresses in the weld center. Compared with the result of MIG welding, the maximum transverse residual stress and the maximum longitudinal residual stress of VPPA-MIG hybrid welding are higher, but the high-stress area of VPPA-MIG hybrid welding are narrower.

Key words: variable polarity plasma arc-metal inert gas; elastic modulus; residual stress; aluminum alloy

Research on image fusion method of visible and near infrared weld pool

FANG Jimi, WANG Kehong, HUANG Yong (Nanjing University of Science and Technology, Nanjing 210094, China). pp 18-23

Abstract: In order to obtain weld pool images with